A.

Sham

X-ray

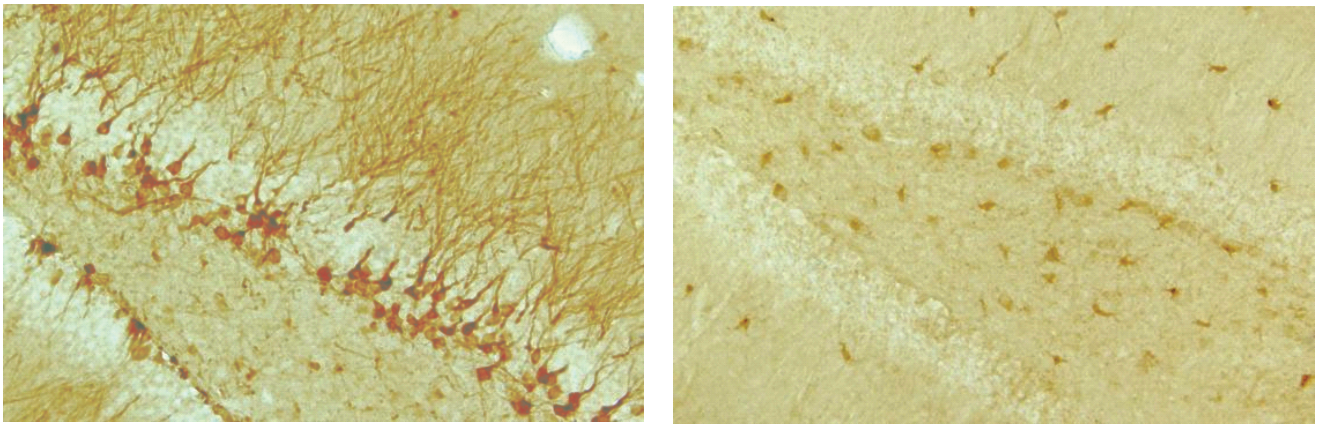

B.

TK -

TK +

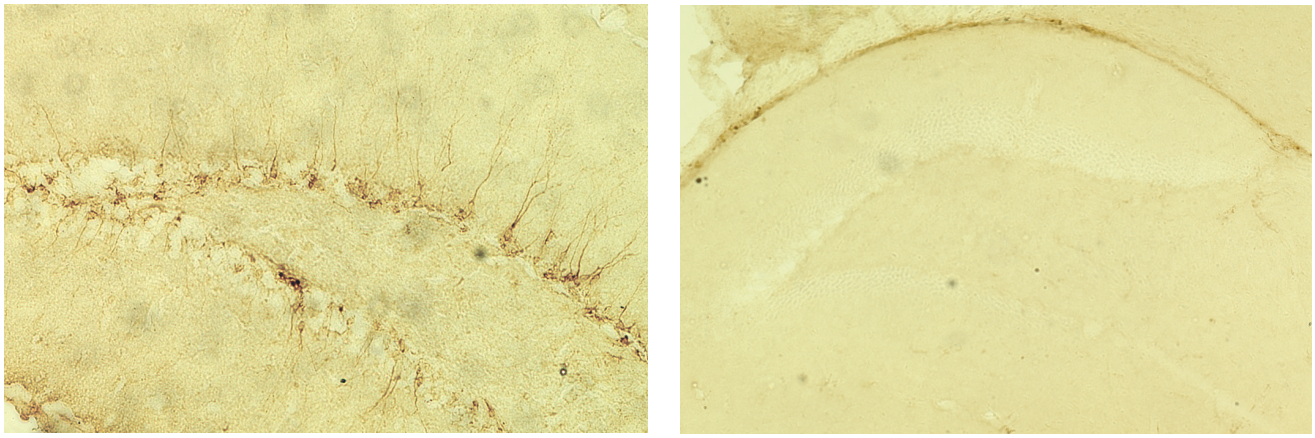

Supplemental Figure 1.
Verifying elimination of adult neurogenesis after X-ray irradiation or the GFAP:TK pharmacogenetic ablation technique: DCX staining for young adult-generated granule cells.
A.) Comparison of DCX staining in sham animals and animals subjected to 3 doses of 5 Gy X-irradiation.
B.) DCX staining in GFAP:TK transgenic animals (right) and wildtype littermates (left), both implanted with ganciclovir minipumps (see Methods section).

Supplemental Figure 2.

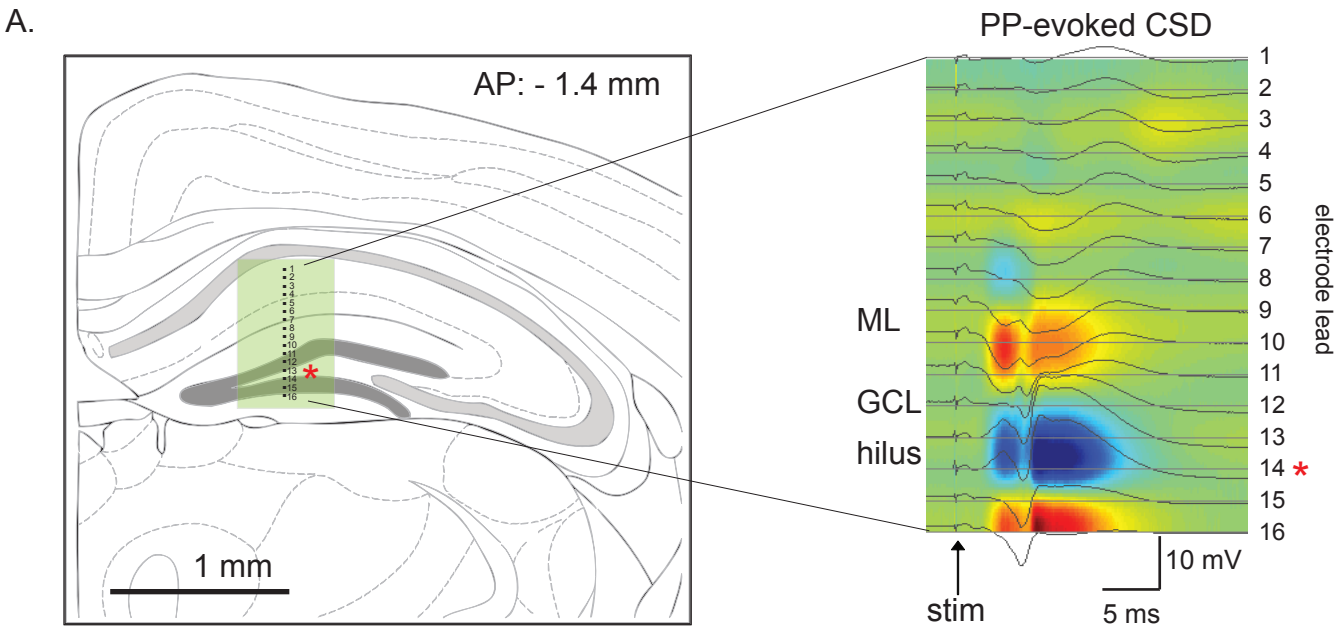

B.

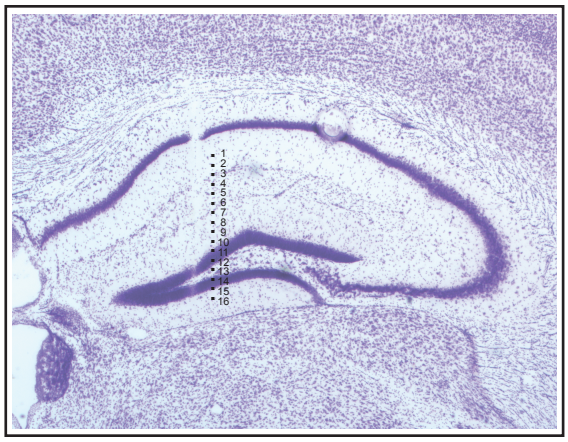

recording electrode track

C.

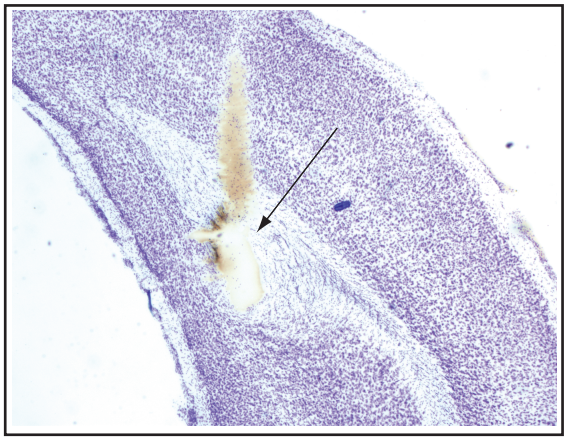

stimulating electrode lesion

Supplemental Figure 2.
Recording and stimulating electrode locations.
A.) Diagram showing range of linear silicon probe recording locations in the dentate gyrus (left; shaded region). Approximate locations of electrode leads along the probe shaft are labeled. A red asterisk marks the probe channel chosen as the hilar electrode for gamma burst analysis. In general, probes were advanced until physiologic reversal of the perforant path evoked field potential were observed on the lower channels of the probe (see PP-evoked LFPs and CSD, right), marking the margin of the free (lower) blade of the dentate granule cell layer.
B.) Representative recording electrode track in a Nissl-stained tissue slice from one animal.
C.) Representative stimulating electrode location. Bipolar concentric stimulating electrodes were lowered to maximize evoked field potential responses in the hilus. Stimulating electrode locations were marked with an electrolytic lesion after completion of recording. (diagram in "A." adapted from "The Mouse Brain in Stereotaxic Coordinates" by Paxinos and Wilson, Elsevier Press)

Supplemental Figure 3.

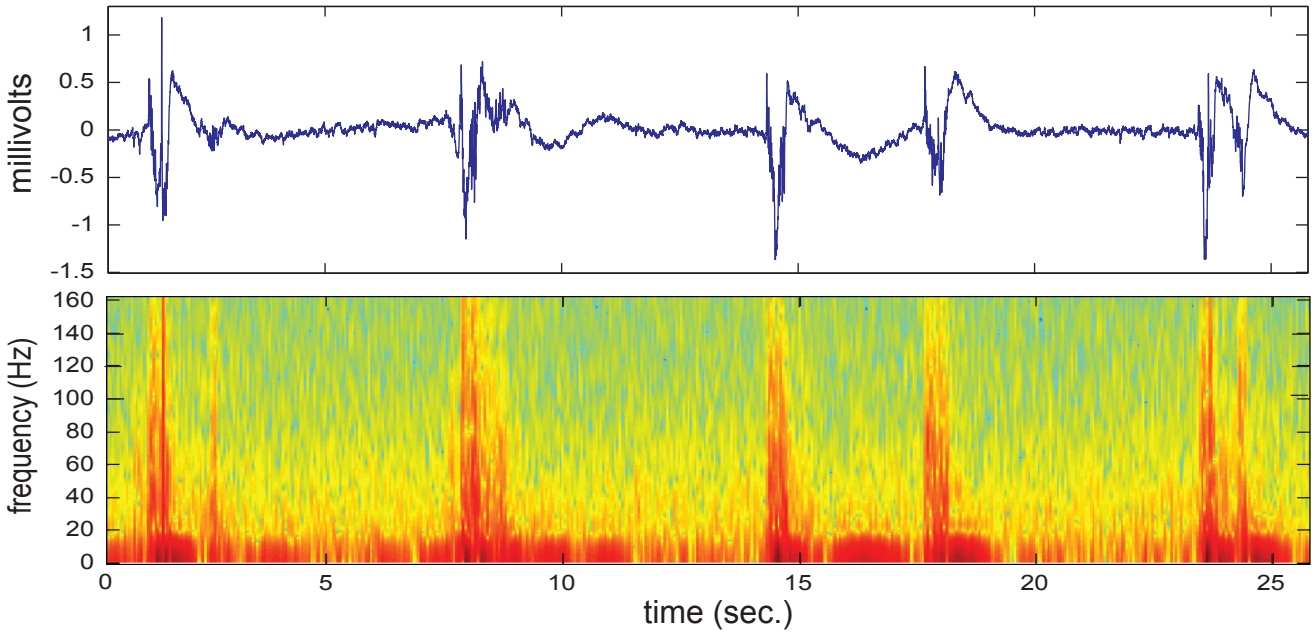

Supplemental Figure 3.
Spectrogram of gamma burst epoch (also shown in Figure 2*a*) showing broad frequency range of bursts.
upper panel: unfiltered LFP from hilar lead of 16-channel linear array.
lower panel: spectrogram of hilar LFP showing broad frequency composition of gamma bursts.

Supplemental Figure 4.

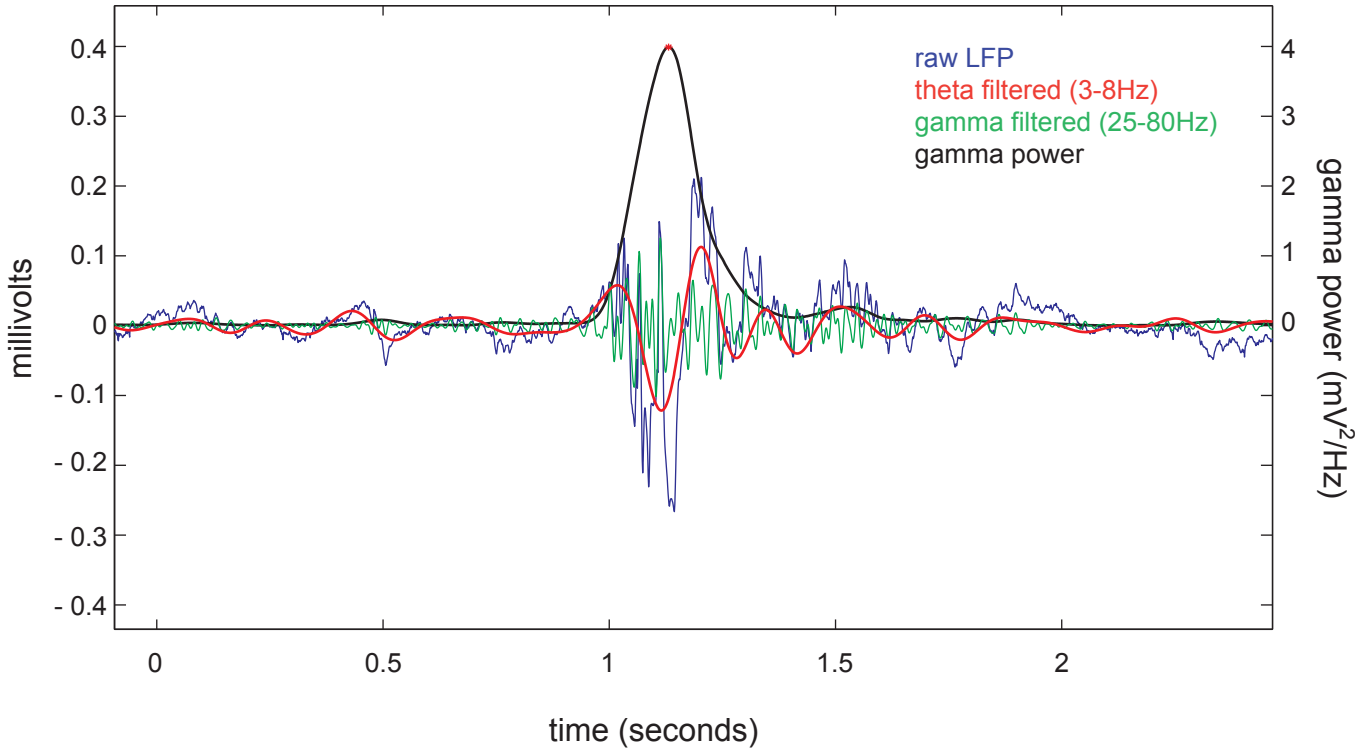

Supplemental Figure 4.
Example of gamma burst detection based upon instantaneous gamma power.
blue: raw LFP from hilus.
red: theta (3-8 Hz) filtered signal.
green: gamma (25-80 Hz) filtered signal.
black: instantaneous gamma power calculated from running average of multi-taper spectrogram.

Supplemental Figure 5.

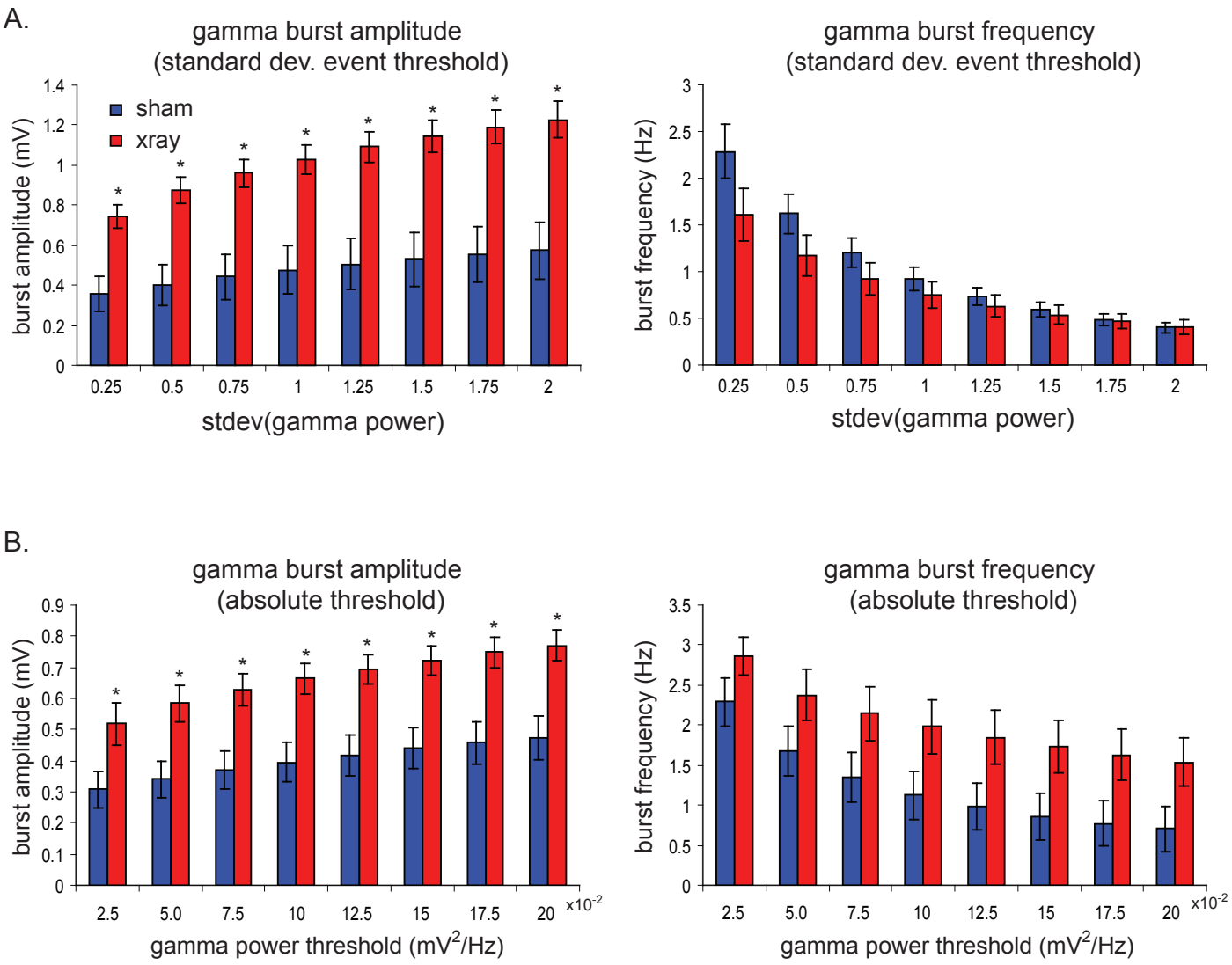

Supplemental Figure 5.
Effect of burst thresholding method on gamma burst statistics.
A.) Gamma burst amplitude and frequency at a range of detection thresholds of instantaneous gamma power based upon the standard deviation of that day's recording.
B.) Gamma burst amplitude and frequency using absolute detection thresholds of instantaneous gamma power ($p<0.05$ for all amplitude comparisons, both methods; $p>0.05$ for all frequency comparisons).

Supplemental Figure 6.

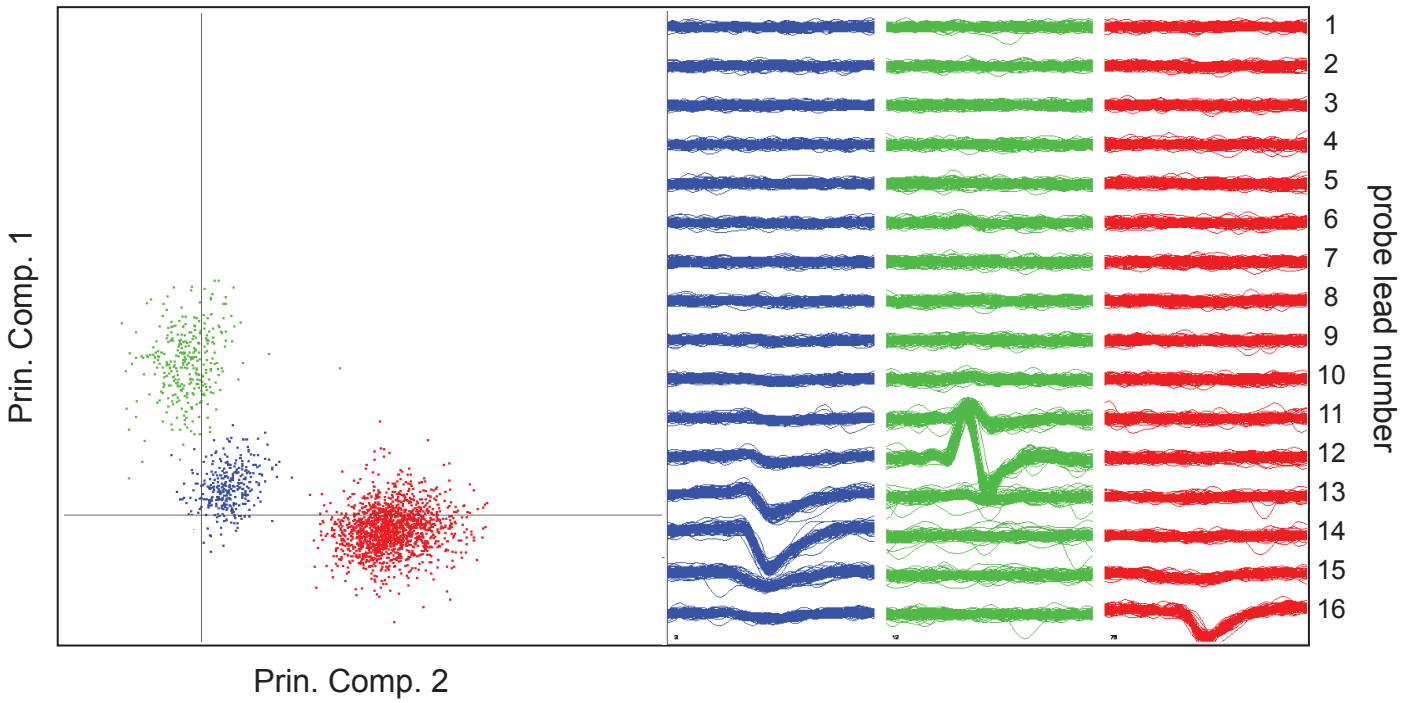

Supplemental Figure 6.
Cluster diagram and waveforms from single-unit isolation.
Cluster diagram (left) shows separation of putative single-units in one animal displayed along two principle components of waveform characteristics. Waveform displays (right) show location of spike waveforms from three putative single-units on the lower channels of the linear silicon probe, positioned in the dentate-hilar region. Clustering was performed using the Klusters software package, Buzsaki lab, Rutgers, NJ.